Applied Acoustics 159 (2020) 107080

Contents lists available at ScienceDirect

Applied Acoustics

journal homepage: www.elsevier.com/locate/apacoust

Influence of texture on tyre road noise spectra in rubberized pavements

L.G. Del Pizzo[a], Luca Teti[b], Antonino Moro[c], Francesco Bianco[b], Luca Fredianelli[a], Gaetano Licitra[c,d,*]

[a] University of Pisa, Physics Department, Largo Bruno Pontecorvo, 3, 56127 Pisa, Italy
[b] IPOOL S.r.l., Via Antonio Cocchi, 7, 56121 Pisa, Italy
[c] CNR – IPCF, Via Moruzzi, 1, 56124 Pisa, Italy
[d] ARPAT – Environmental Protection Agency of Region of Tuscany, Area Vasta Costa, Via Marradi 114, 57125 Livorno, Italy

ARTICLE INFO

Article history:
Received 11 January 2019
Received in revised form 17 September 2019
Accepted 29 September 2019
Available online 22 October 2019

Keywords:
Tyre/road interaction
Tyre/road noise
CPX measurements
Road texture
Modelling

ABSTRACT

Road traffic noise is the most common source of environmental pollution in urban areas and therefore, the study of noise mitigation actions is fundamental for urban planning. The main source of road traffic noise is tyre/road interaction; thus, the use of low noise road surfaces represents an optimal solution for its mitigation. Several studies tried to find a correlation between road texture and broadband noise data, trying to provide guidelines for the development of acoustically optimised road surfaces.

The present work studies the correlation between road texture and tyre/road noise from an experimental point of view, by analysing texture and noise spectra on ten different road surfaces. Tyre deformation has also been addressed by analysing two already existing tyre envelopment algorithms. The first algorithm, proposed by Von Meier and based on the limitation of the second order derivative of the profile signal, shows poor correlation with high frequency noise, while the second algorithm, based on a novel method proposed by Sandberg and Goubert and called indenter method, enhances correlation with low frequency noise and preserves information at higher frequencies. Correlation patterns show that rolling noise can be separated in three main contributions: low, middle and high frequency noise. Finally, experimental tyre/road noise and enveloped texture data obtained with the indenter algorithm have been used to elaborate a linear model that relates low and high frequency noise to texture one-third octave bands. This model deepens knowledge on tyre/road interaction.

1. Introduction

Noise pollution produced by transport infrastructures is a very widespread issue for modern society, especially for the inhabitants of urbanized areas. Despite the efforts of the scientific community to study new mitigation measures, the recent European Environmental Noise Directive revision [1] reported that noise pollution continues to be a major health problem in Europe. Even if not the most annoying, road traffic is the most common noise source and about 100 million people in the 33 EU member states are exposed to harmful road traffic noise levels exceeding 55 dB(A) of L_{den}, and 32 million are exposed to noise levels higher than 65 dB(A) of L_{den}. An exposure to such high noise levels could lead to a whole list of health effects, such as: sleep disorders with awakenings [2], learning impairment [3,4], hypertension ischemic heart disease [5] and annoyance [6]. The prevention of such effects is remanded to mandatory action plans for big infrastructures or urban agglomerations [7], and in order to optimize mitigations [8], noise generation mechanisms are of paramount interest.

Studies show that road traffic noise is a remarkably complex phenomenon, with different sources such as the power unit, aerodynamics and tyre-road interaction [9,10], which constitutes the most important source of traffic noise, particularly for traffic speeds that range from 35 up to 120 km/h. Noise caused by tyre/road interaction shows a strong degree of variability, depending on properties of both tyre and pavements, since its generation mechanisms involve several mechanisms that occur simultaneously.

A combination of aerodynamic and vibro-dynamic phenomena occurs in the generation of tyre/road noise, where the contact between tyre and pavement acts as a source [11]. Aerodynamic noise is related to compression of the air trapped within the tread of the rolling tyre [12,13]. This mechanism is known as air pumping and causes noise at frequencies higher than 1 kHz. Other than air pumping, aerodynamic mechanisms also include pipe and Helmholtz resonances [14], due to the coupling of a vibrating mass of air within the tread, which acts as a cavity [9].

* Corresponding author.
E-mail address: g.licitra@arpat.toscana.it (G. Licitra).

https://doi.org/10.1016/j.apacoust.2019.107080
0003-682X/

Vibro-dynamic noise covers frequencies lower than 1 kHz, and is due to tyre vibrations caused by the impact of the tyre against irregularities of the road surface. It is also caused by non-linear effects such as the stick-and-slip and stick-and-snap mechanisms [15]. While the former is caused by the motion of the tyre treads with respect to the road surface, the latter is present when the grip on the tyre is too strong, as it can happen on newly laid road surfaces [9].

The three main dominions (generation, absorption, propagation) which affect pavement acoustic performance involve a number of acoustic parameters [16]: in fact, a comprehensive approach for the evaluation of noise at receivers must analyse not only the generation mechanisms of traffic noise, but propagation and absorption-reflection processes that can occur during propagation [10].

In this paper, however, tyre/road noise is studied only in relation to road texture, since the aim is to propose a phenomenological model of the source based on measures performed according to the CPX method defined by ISO 11819-2 [17] as a function of road texture.

2. State of the art

The description of tyre/road interaction carried out by Sandberg [9] has led to the separation of aerodynamic and vibrational contributions, raising awareness about the fundamental properties of road surfaces related to noise generation. In particular, surface macro and megatexture, as defined by ISO 13473-2 [18], porosity and layer thickness play a key role in generation of rolling noise [19].

ISO 13473-2 defines road texture as the deviation of a pavement surface from a true planar surface, caused by the random disposition of the surface elements and their superficial roughness. Wavelengths from 0.5 mm to 50 mm are addressed as macrotexture, while longer wavelengths, up to 50 mm, form megatexture. Macrotexture covers wavelengths that are the same order of size as tyre tread elements, while megatexture is of the same order of size as tyre-road interface.

A common approach to studies concerning road texture is provided by spectral analysis in constant-percentage bandwidth, using octave bands or one-third octave bands defined by ISO 13473-4 [20].

Sandberg's studies [9] underlined that the lower range of macrotexture, which includes wavelengths shorter than 10 mm, is negatively correlated with high frequency noise; conversely the first part of megatexture, up to 80 mm, shows a strong positive correlation with low frequency, vibrational noise. These studies led to the definition of the Estimated Road Noisiness Level (ERNL), an estimation of roadside broadband noise, as a linear combination of the octave bands centred in 5 mm and 80 mm.

Using a similar approach, Losa et al. [6], within the framework of the Leopoldo project [21], proposed a model that estimates broadband rolling noise measured with the CPX method as a linear combination of texture levels within 2–4 mm and 16–63 mm. While the former is positively correlated with noise emission, the latter shows a negative correlation.

ISO 13473-5 [22] suggests using the texture level in the octave band centred at 63 mm as an indicator of tyre/road noise, since these wavelengths correspond approximately to the length of the interface between tyre and road.

A study based on sieve analysis of the aggregates that form the road surface has shown that only the diameter of the 95% passing sieve is positively correlated with noise generation, while a negative correlation links noise and void percentage [19]. This study, although focusing on properties of road pavements other than texture, underlines yet again the presence of two generation mechanisms. Despite the simple linear relations found in the study, the resulting model requires pavement coring in order to obtain data and therefore is not so practical for spatial evaluation conducted for each site.

Models of rolling noise based on FEM and BEM approaches have been proposed to describe tyre vibrations. These models are mainly based on the decomposition of tyre simulation in three components: a non-linear stationary rolling case, an eigenvalue analysis on a deformed tyre model and a noise radiation prediction module [23,24]. These approaches, however, are more focused on optimising acoustical design of tyres, and are therefore less interesting as far as this work is concerned.

A simple evaluation of texture does not distinguish between positive texture, i.e. when a road surface is characterised by high peaks, and negative texture, where deep grooves and valleys are dominant [25]. In fact, possible asymmetry of the profile is not evident by an abrupt spectral analysis, which does not distinguish between ridges and valleys of equal amplitude. It has been reported that negative texture results on a decrease of rolling noise, while positive texture is more aggressive from an acoustical point of view.

It is therefore evident that tyre/road noise modelling based only on an abrupt evaluation of texture spectrum would erroneously conclude that pavements with equal spectra are acoustically identical [26], while, on the other hand, an experimental study of the relationship between road texture and rolling noise that does not take into account the difference between positive and negative texture would lead to the wrong conclusion that rolling noise exhibits random variations for road surfaces with same texture spectra.

The measure of asymmetry of a profile is provided by the skewness, defined as the ratio of the mean value of the cube of the profile and the cube of the standard deviation.

When a tyre runs on a textured road surface with high negative skewness, it does not necessarily touch all the points on the surface, and, therefore, tyre envelopment of the road surface can be used to distinguish road surfaces with different skewness.

Several algorithms that simulate the deformation of the tyre due to the contact with the road surface have been developed. The first algorithm that simulates tyre envelopment was developed by Von Meier. Von Meier's method (VM), was based on empirical and heuristic considerations [27], such as the limitation of the second-order derivative of the profile signal. Other methods are based on the analytical solution of the tyre deformation due to the roughness of the road surface, such as the method proposed by Hamet and Klein which describes the tyre-road system using the Green function [25]. The solution proposed approximates the tyre as a two-dimensional infinite elastic medium; moreover, the resulting integral equation is never exactly solved, and relies on an iterative approach.

Sandberg and Goubert derived an envelopment procedure based on experimental analysis of the behaviour of the SRTT used for CPX measurements [28]. This study shows that the tyre envelopment follows the road profile until a certain depth, determined by the kind of tyre and the speed of the vehicle.

3. Methods and sites analysed

Noise and road texture measurements were carried out during November 2017 on ten different sites of the highway connecting Merano to Bolzano, located in the region of Trentino-Alto Adige/Südtirol in Northern Italy. Since the maximum distance between sites is about 20 km and the difference in height at the starting and ending point of the highway is about 100 m, it is safe to assume that the sites are exposed to the same weather and traffic condition, minimising ageing influence on measurements [29,30].

A complete flowchart of the paper's experimental plan is proposed in Fig. 1.

The characteristics of each site in terms of aggregate gradation of the ten pavements are reported in Fig. 2. As summarised in Table 1, sites from P1 to P4 and P7 are gap graded 0/12 rubberized asphalts, produced according to the *dry* process, while sites P5, P6, P8 and P9 are gap graded 0/16 rubberized asphalts produced following the *wet* process. P10 is a dense asphalt concrete 0/12.

It is useful to remind that rubberized road surfaces are built using hot asphalt mixes containing crumb rubber which acts as a modifier, in order to improve the acoustical properties of the binder [31]. In the wet process, named *Asphalt Rubber* (AR), crumb rubber is blended with liquid asphalt cement (AC) before mixing AC with the aggregate; in general, the percentage of crumb rubber used in this process is roughly equal to 1% of the total weight. In the dry process, crumb rubber is added to the hot aggregate, usually in the range of 1–3% of the weight of the total mixture before adding the AC.

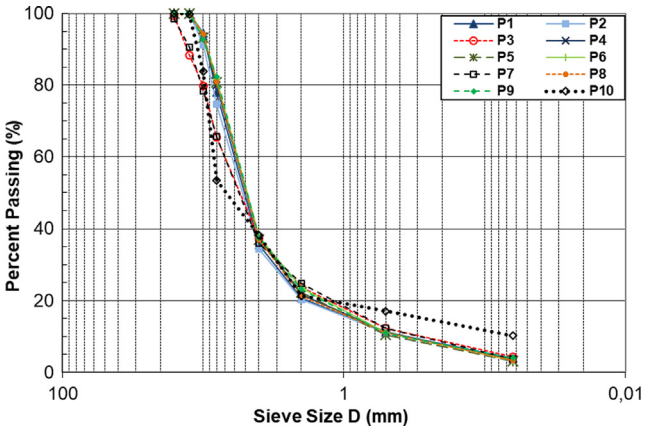

Fig. 2. Aggregate gradations of pavements analysed.

3.1. Noise measurements

In this work, a modified protocol based on the CPX method [32,33] was used for evaluating tyre/road noise. Measurements are compliant to the last version of ISO 11819-2 [17], since Standard Reference Test Tyre (SRTT) was used and temperature and hardness normalisations were also performed using a reference temperature of 20 °C and reference hardness of 66 Shore A. The reference speed adopted for the calculation of CPX levels is 100 km/h.

During the measurement sessions, several acquisition on the same surface were performed, varying the speed at each run. A minimum χ^2 iterative algorithm is used in each segment for fitting sound levels with speed, in order to compute the one-third octave bands spectrum at the reference speed. Finally, the mean value of the sound pressure level within each band is used to characterise the whole site. As per ISO requirements, for each road surface, the broadband noise level L_{CPX} expressed in dB(A) is calculated by summing all the A-weighted energy contributions $L_{CPX,i}$ within the 13 bands from 315 to 5000 Hz. Indicating with A_{weight} the value of the A-weighting curve, the broadband level is given by (1):

Table 1
Sites surveyed and their characteristics.

Road Surface	Road Type	Road Surface	Road Type
P1	Dry gap-graded 0/12	P6	Wet gap-graded 0/16
P2	Dry gap-graded 0/12	P7	Dry gap-graded 0/16
P3	Dry gap-graded 0/12	P8	Wet gap-graded 0/16
P4	Dry gap-graded 0/12	P9	Wet gap-graded 0/16
P5	Wet gap-graded 0/16	P10	Dense Asphalt Concrete 0/12

$$L_{CPX} = 10\log\sum_{k=1}^{13} 10^{0.1(L_{CPX,i}+A_{weight})} \quad (1)$$

The uncertainties related to broadband levels resulting from Eq. (1) are estimated using propagation based on maximum error of the uncertainties on each one-third octave band $\Delta L_{CPX,i}$ derived from the fitting algorithm according to Eq. (2):

$$\Delta L_{CPX} = 10\log\frac{\sum_{k=1}^{13} 10^{0.1(L_{CPX,i}+A_{weight}+\Delta L_{CPX,i})}}{\sum_{k=1}^{13} 10^{0.1(L_{CPX,i}+A_{weight})}} \quad (2)$$

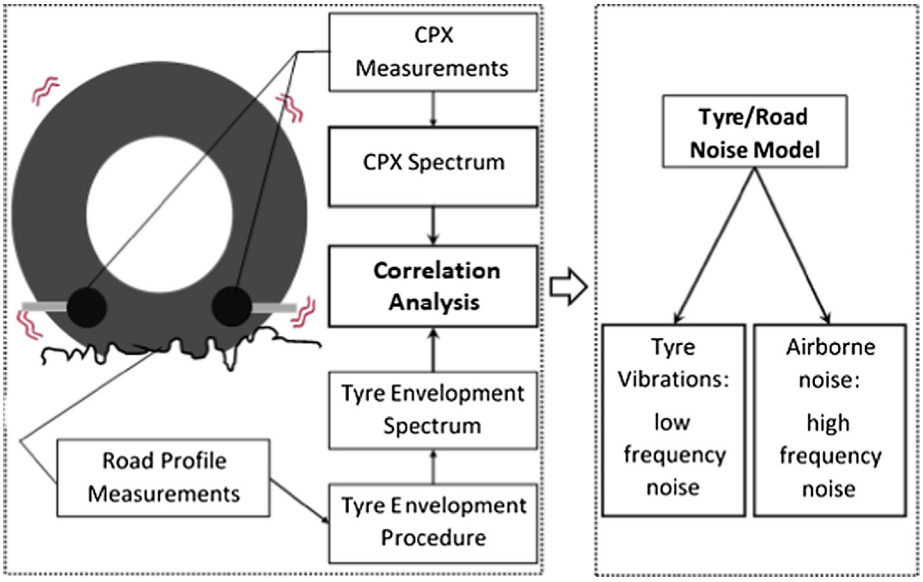

Fig. 1. Flowchart of the paper's experimental plan.

The main modification to the official protocol regards data analysis, since the test sites were divided in segments 6.18 m long, i.e. three times a tyre circumference, instead of using the standard section length of 20 m, in order to increase the spatial resolution of the analysis.

3.2. Road texture measurements

Road texture measurements were carried out at the same time as CPX measurements, using a triangulation point profile sensor, compliant with the requirements reported in ISO 13473-2 [18]. The set-up is based on a measurement system mounted on a self-powered vehicle, where the CPX equipment and the profilometer for texture measurements are deployed at once. In this way, both CPX and road texture measurements are carried out at the same time, thus ensuring perfect alignment of signals and same conditions of measurement.

According to the terminology adopted by ISO 13473-2 [18], the profilometer used during measurements is a contactless profilometer, based on the setup described in [34]. It combines the output of the laser sensor fixed to the rear of the vehicle, a piezoelectric accelerometer that measures vertical oscillations of the sensor and a rotary encoder fixed to a wheel that yields the horizontal distance travelled. The information provided by the rotary encoder is then used to obtain a profile with sampling distance of 0.5 mm.

The resulting profiles were divided in adjacent segments. Since measurements of noise and texture are performed simultaneously, the profile segments result aligned to the CPX measurements.

In order to reduce noise in the profile signal, in each segment the profiles were fitted with an autoregressive model based on the Yule-Walker method. Then, texture spectra are calculated using power spectral density and adding the energy within each one-third octave bands, following the prescriptions of the fourth method reported in ISO 13473-4 [20].

Since our analysis focused on tyre envelopment procedures, which are linked to noise induced mainly by tyre vibrations, texture spectra were calculated from 5 to 200 mm. It is known, in fact, that shorter wavelengths are connected to aerodynamic phenomena, while wavelengths that range in megatexture are responsible for in-vehicle noise, passenger comfort and ride quality [9,22].

3.3. Measurement uncertainty and spatial variability

The uncertainty related to the mean CPX values, named L_{CPX} hereafter, derives from three main contributions. The first source of uncertainty derives from the fitting process in each segment, due to data dispersion around the fit. Since the dispersion around the fit is assumed to be a random source of error, it is assumed to be the measurement uncertainty of the sound pressure level within the given segment.

The uncertainty of the mean value of the CPX sound pressure level within a band can be evaluated taking into account the spatial homogeneity of the installation, i.e. data dispersion around the mean value. Spatial homogeneity, represented by the standard deviation of L_{CPX} data on a road surface, is a description of the mean value precision and it cannot be neglected when two road surfaces are compared [32].

The last source of data variability derives from "several factors and processes, whose cause and nature of disturbance are either known, but randomly distributed in an uncontrollable way, or are of a systematic nature, but affect the result in an unpredictable way" (as declared in Annex K of the ISO 11819-2). Since measuring conditions do not vary greatly within the different sessions, this source was neglected in the analysis.

The same reasoning applies to road texture spectra: in each segment, a measurement uncertainty of the segment spectrum was derived for each one-third octave band, assuming that the signal within a band has the same properties as white Gaussian noise.

In fact, as well known [35], the uncertainty Δz^2_{SEG} related to the RMS value of a bandwidth-limited white Gaussian noise $z(x)$ with bandwidth Δk and length L can be evaluated according to the Eq. (3):

$$\Delta z^2_{SEG} = \frac{\sigma^2\{z(x)\}}{\sqrt{\Delta k L}} \tag{3}$$

where $\sigma^2\{z(x)\}$ is the variance of the random process $z(x)$. Since the profile $z(x)$ is filtered to yield a zero-mean and zero-slope signal, its variance in a band centred in k is also equal to the mean square value$Z^2_{SEG}(k)$:

$$\Delta z^2_{SEG}(k) = \frac{Z^2_{SEG}(k)}{\sqrt{\Delta k L}} \tag{4}$$

Propagation of maximum error in dB provides an estimate of measurement uncertainty for texture levels within the band centred in k $\Delta L_{txSEG}(k)$ of each segment:

$$\Delta L_{txSEG}(k) = 10\log\left(1 + \frac{1}{\sqrt{\Delta k L}}\right) \tag{5}$$

Data dispersion around the mean value is taken into account by computing the sample standard deviation due to spatial variability and performing quadratic addition with the resulting estimates of uncertainty provided by Eq. (5).

3.4. Road texture envelopment method

Since only the portion of road profile that is in contact with the tyre is directly involved in rolling noise generation, several algorithms capable of simulating the deformation of the tyre due to the contact with road texture have been developed. The two methods compared in this work are Von Meier's method (VM) [27] and the indenter method by Sandberg and Goubert (SG) [28].

Von Meier's studies represent the first attempt to simulate the tyre envelopment of road texture. This method is based on the limitation of the second-order derivative of the signal given by Eq. (6), in order to simulate the tyre rubber deformation due to the contact with the road surface.

$$\frac{2z_i - z_{i-1} + z_{i+1}}{dx^2} \le d^* \tag{6}$$

where:

z_i is the discretised profile;
d^* is the maximum value of the second difference, equal to $0.054\ \mathrm{m}^{-1}$ as suggested by Von Meier;
dx is the sampling distance.

The procedure is carried out iteratively raising or lowering each point of the profile of a fixed quantity, depending on the difference between the value of the second order derivative in that point and the threshold chosen. The process halts when the condition provided by Eq. (6) is verified for each profile point. The parameter d^* is related to tyre hardness, with lower values simulating higher hardness; for instance, a soft tyre can be modelled by choosing a limit value of $0.1\ \mathrm{m}^{-1}$, while a stiff tyre would provide $d^* = 0.01\ \mathrm{m}^{-1}$.

The indenter method has been derived by Sandberg and Goubert from measurements of a known profile filled with plasticine and run over by a car tyre. As the tyre rolls on the profile, it presses out the plasticine, leaving only the modelling clay that covers the volume between the tyre rubber and the profile.

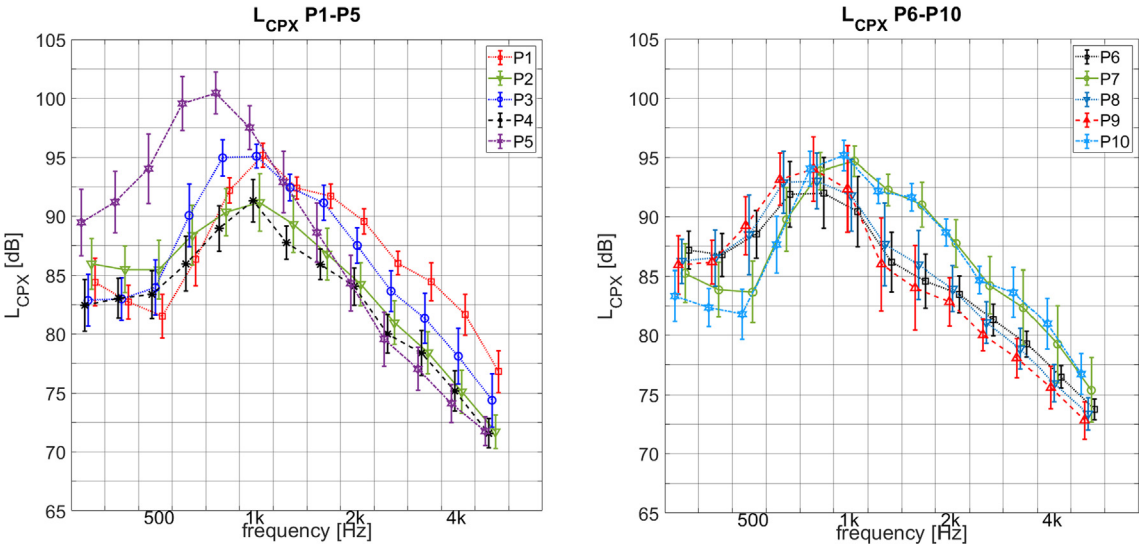

Fig. 3. Mean L_{CPX} spectra for the road surfaces analysed.

Table 2
Mean broadband CPX levels and related uncertainty.

Road Surface	Broadband Level [dB(A)]	Road Surface	Broadband Level [dB(A)]
P1	100.5 ± 0.6	P6	97.4 ± 1.3
P2	97.2 ± 1.2	P7	100.6 ± 0.9
P3	100.7 ± 0.8	P8	98.4 ± 1.3
P4	96.3 ± 0.9	P9	98.5 ± 1.4
P5	104.2 ± 1.1	P10	100.6 ± 0.7

The results show that for two-dimensional profiles, a tyre envelopment can be simulated by indenting an area S into the rubber of the tyre. This area does not depend on texture characteristics, but only on tyre properties, i.e. tyre pressure, width and speed.

The code developed to perform the indenter method is based on the guidelines present in [28], along with the values of the indented area for the SRTT ($S = 5$ mm^2) and includes the following steps:

1. The profile is divided into footprints of fixed length L, representing the length of the tyre/road contact zone;
2. For each footprint, a horizontal line, starting from $z = z_{max}$ is iteratively lowered until the area A under the profile and above this line reaches the predefined value S;
3. Evaluation of the points indented inside the rubber proceeds to the next footprints, until the last one is reached;
4. Points above the line for each footprint are kept in the enveloped profile, while the points below are excluded from the profile;
5. Interpolation between adjacent indenters is provided by a Piecewise Cubic Hermite Interpolating Polynomial (PCHIP).

Even though measurements were not carried out at the reference speed of 100 km/h chosen in this work, it is reasonable to assume that the indented area does not vary significantly, at least on a first approximation.

4. Analysis and results

4.1. Noise measurements

Since measurements were performed using the reference tyre SRTT proposed by ISO/TS 11819-3 [36], tyre properties, such as

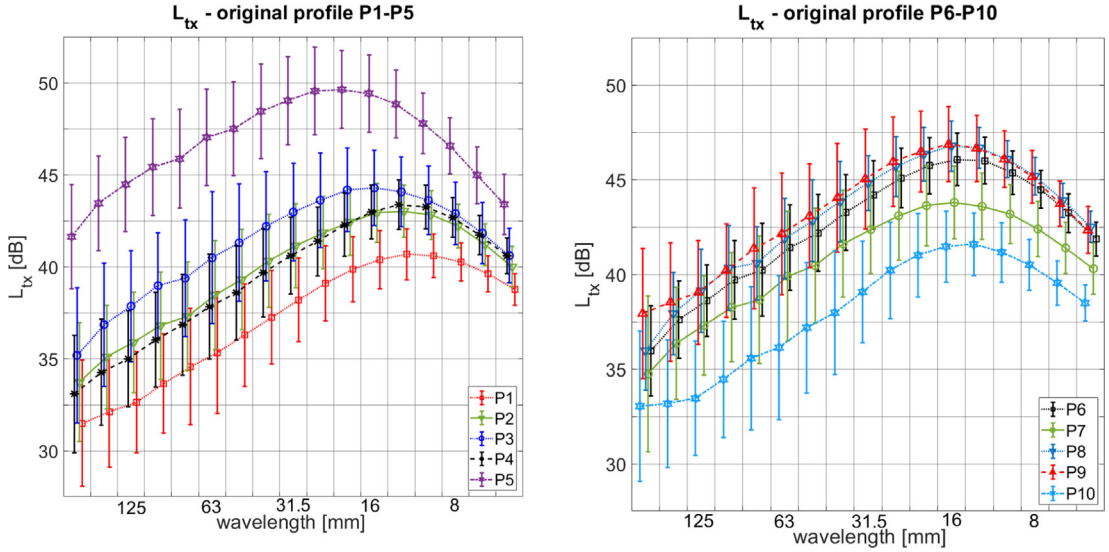

Fig. 4. Road texture spectra.

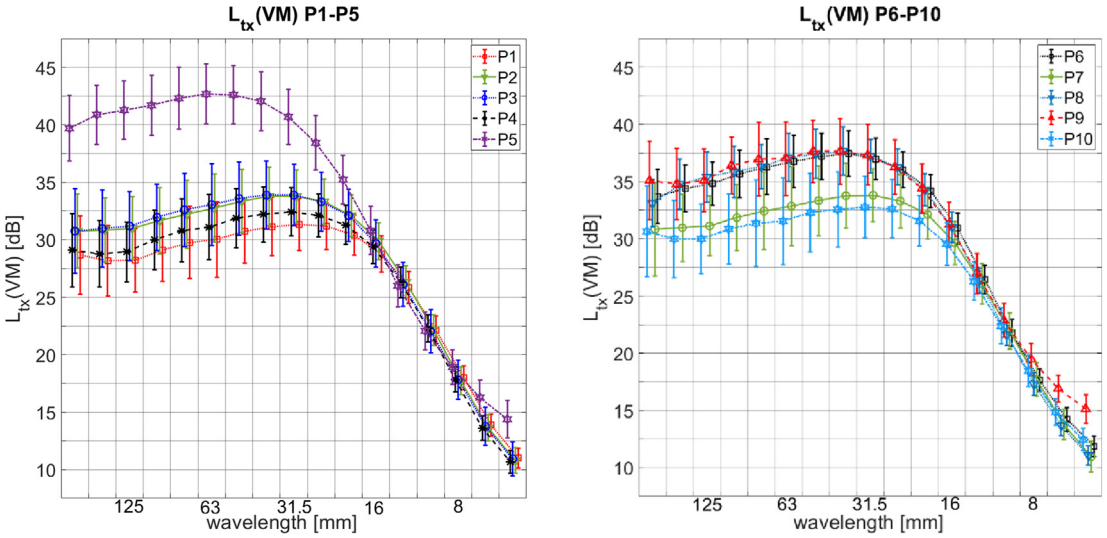

Fig. 5. Texture spectra resulting from VM method.

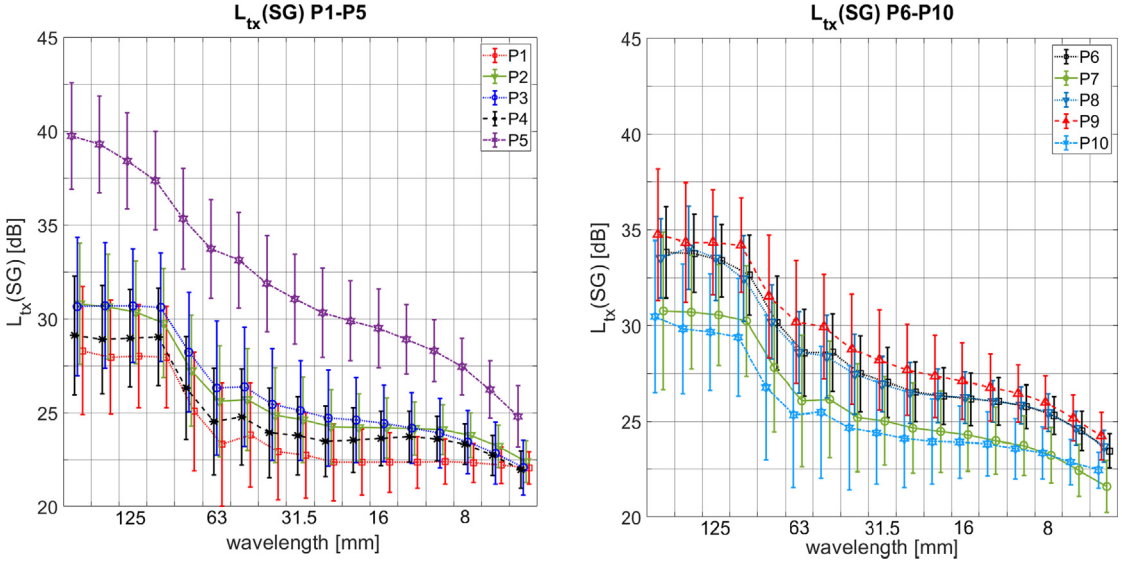

Fig. 6. Texture spectra resulting from SG method.

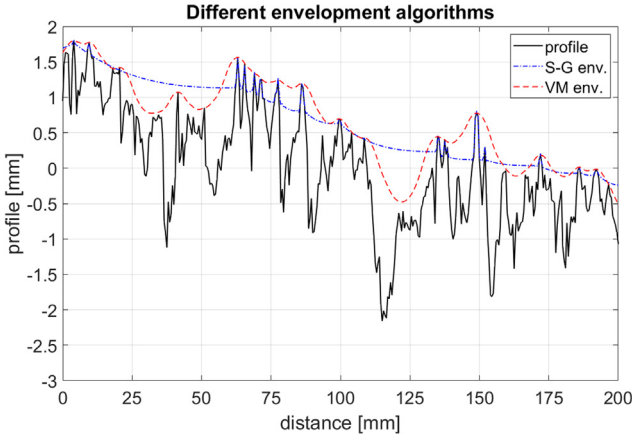

Fig. 7. Comparison of envelopment algorithms.

rubber type, tread pattern, tyre pressure and its diameter, were not investigated, despite other studies underline their influence on acoustical emission [37]. Nevertheless, since the focus of the study is the relation between road texture and tyre/road noise, using the same tyre for all road surfaces minimises the number of uncontrolled variables within the study.

Mean CPX spectra and their related uncertainties are shown in Fig. 3, while L_{CPX} broadband levels calculated using Eqs. (5) and (6) are reported in Table 2.

4.2. Road texture measurements

Following the protocol reported in ISO 13473-4 [20], texture spectra were calculated as a function of wavenumber however, for the sake of clarity, results are plotted as a function of wavelength, its inverse.

Texture spectra were evaluated for road profiles and tyre envelopments, allowing a comparison of the results. VM algorithm

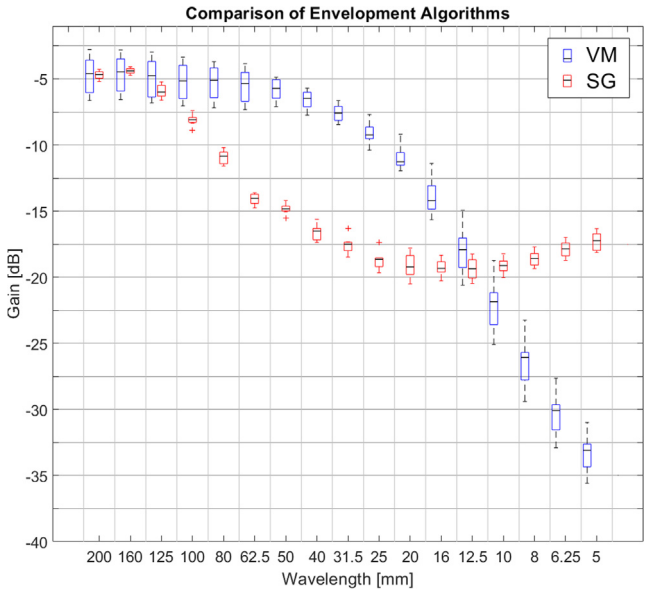

Fig. 8. Comparison of VM algorithm and SG algorithm.

mainly affects short wavelengths and does not alter longer wavelengths; on the contrary SG texture levels do not show such a sharp cut-off. The lower texture levels of SG profiles compared with the levels of original profiles, can be explained by the overall reduction of profile amplitudes.

While Fig. 4 shows texture spectra calculated form road profile measurements, Figs. 5 and 6 show texture spectra resulting from the tyre envelopment process, according to VM and SG method.

An example of the measured profile and the resulting tyre envelopments provided by the two methods is shown in Fig. 7.

The response of the envelopment algorithms was evaluated by calculating the gain function, viz. the ratio between the spectra of the enveloped and original profiles. Boxplots of the gain function, reported in Fig. 8, show the different behaviour of the two envelopment algorithms as a function of texture wavelength. The two algorithms exhibit different trends: while VM procedure mainly acts as a low pass filter, SG indenter method does not show such a sharp cut-off.

4.3. Correlation between road texture and rolling noise

As far as the relation with rolling noise is concerned, correlation patterns between each couple of texture and noise one-third-octave bands were calculated for original profiles, VM profiles and SG profiles. The correlation patterns between the texture levels of the original profile and rolling noise, shown in Fig. 9(a), are in accordance with previous studies, which define two distinct well-correlated zones: a positive, low frequency zone and a negatively correlated high frequency zone.

Positive correlation is slightly enhanced using SG algorithm, whose correlation pattern with noise is shown in Fig. 9(b), with a slight decrease of negative correlation in the high frequency region, compared to the original profile.

While preserving low frequency correlation with long texture wavelengths, VM algorithm shown in Fig. 9(c) alters the behaviour of the one-third-octave band centred in 10 mm, producing a low correlation line, and significantly reduces the correlation at shorter wavelengths. Negative correlation with high frequency noise results also significantly diminished.

Therefore, only SG algorithm results suitable for creating a model of rolling noise that takes into account tyre deformation due to road profile.

The correlation patterns shown in Fig. 9(a), (b) and (c) confirm the existence of different regions for the profile and the tyre envelopments:

1. A low frequency region, which involves the range from 315 to 800 Hz, positively correlated to road texture and with a maximum at 80 mm;
2. A high frequency region, from 2000 to 5000 Hz, negatively correlated to road texture, with a minimum at 8 mm;
3. A middle frequency region, where the transition from positive to negative correlation occurs.

While the low frequency and high frequency regions show well defined correlations, the middle region shows almost no correlation with road texture.

4.4. Low and high frequency CPX indicators

Since the relationship between noise and texture can be separated in two different well-correlated regions, with a slow transition occurring at frequencies around 1 kHz, two new variables were created from the one-third octave bands noise level: the low frequency noise level $L_{CPX}(LF)$, which includes frequencies from 315 to 800 Hz, and the high frequency noise level $L_{CPX}(HF)$, which includes noise from 2000 to 5000 Hz:

$$L_{CPX}(LF) = \sum_{j=315}^{800} 10^{0.1 L_{CPX}(j)}$$

$$L_{CPX}(HF) = \sum_{j=2000}^{5000} 10^{0.1 L_{CPX}(j)}$$

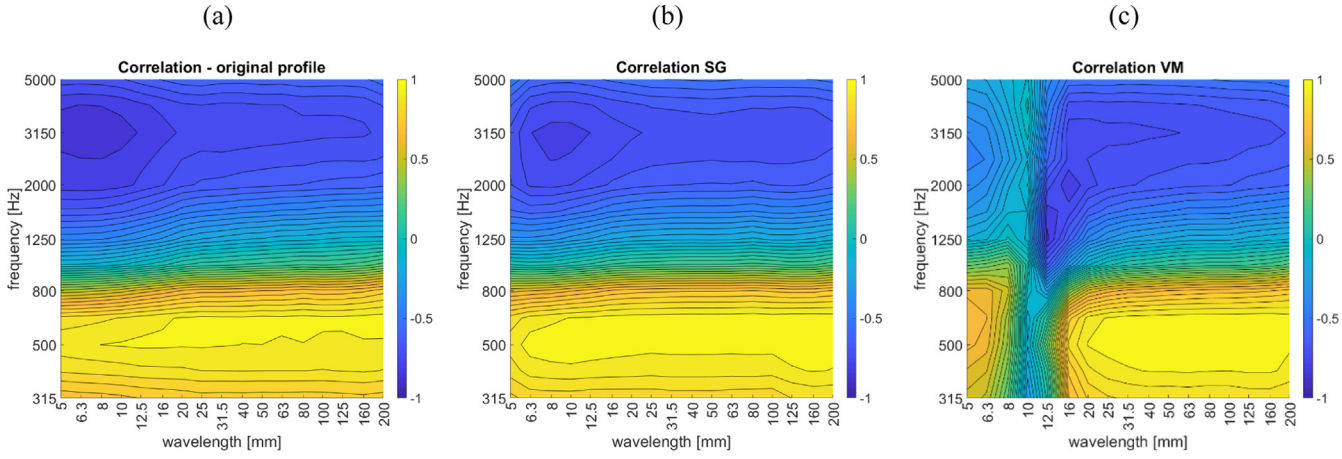

Fig. 9. Correlation coefficient between road texture and noise one-third-octave bands, for the original profile (a), the SG enveloped profile (b) and the VM profile (c).

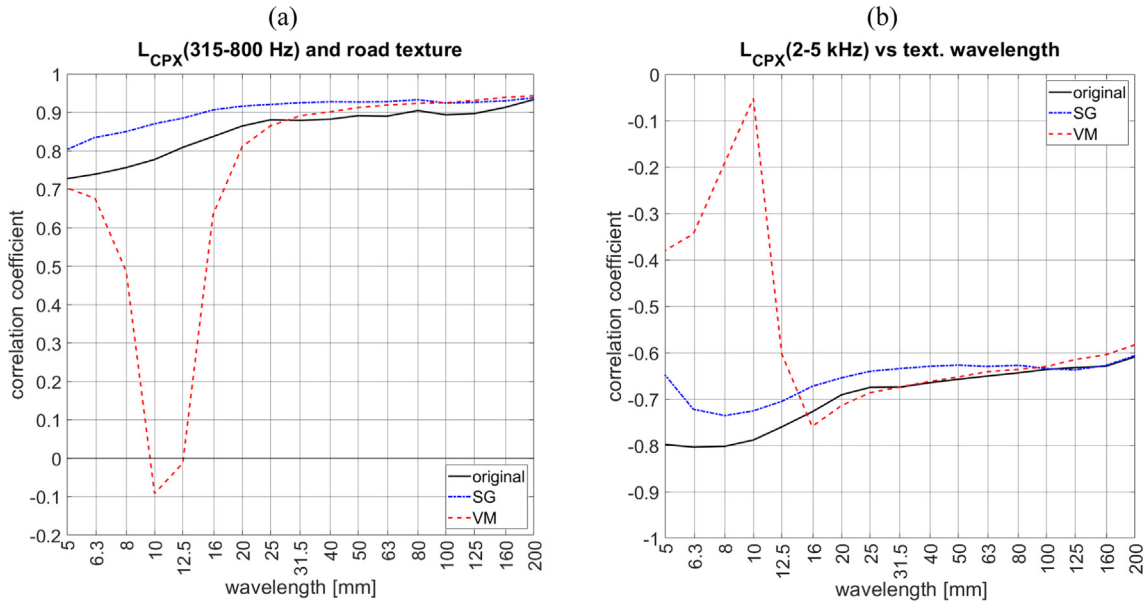

Fig. 10. Correlation curves of low frequency (a) and high frequency (b) noise and texture levels. The ordinate axes are on different scales to improve readability.

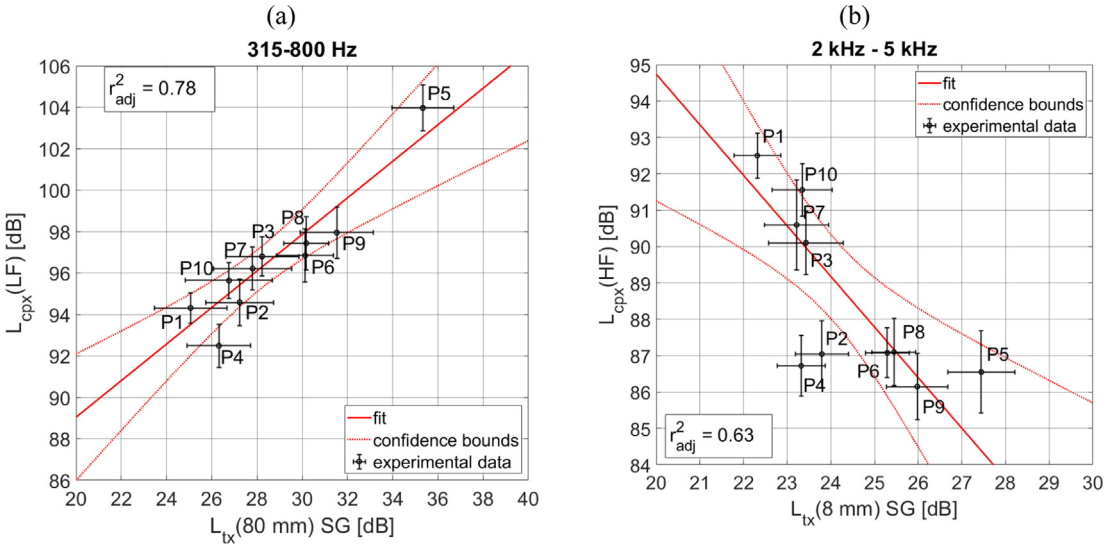

Fig. 11. Linear fit of data with complete dataset.

Table 3
Regression parameters for low frequency noise.

Number of data points	a_{hf}	b_{hf}	Adj. r^2
10	0.88 ± 0.15	71.4 ± 4.3	0.78
7	0.56 ± 0.07	80.5 ± 2.0	0.91

Table 4
Regression parameters for high frequency noise.

Number of data points	a_{bf}	b_{bf}	Adj. r^2
10	−1.39 ± 0.34	122.5 ± 8.4	0.62
7	−1.77 ± 0.11	132.2 ± 2.7	0.98

Correlation coefficients between these parameters and texture one-third-octave bands were recalculated for the road profile and the two tyre envelopments. The results, shown in in Fig. 10(a) and (b), underline that envelopment algorithms enhance positive correlation with low frequency noise, but provide a different response for high frequency noise: while the SG algorithm exhibits the highest negative correlation at 8 mm, VM algorithm shows almost no correlation at these wavelengths.

Moreover, correlation curves in Fig. 10(a) and (b), show that low frequency rolling noise is related to the whole range of road texture wavelength, rather than to a single wavelength band; conversely high frequency noise is rather peaked around 8 mm, especially after SG enveloping.

Despite the correlation between noise and road texture shows small variation with road texture wavelength, it is still possible to determine the texture bands that correlate the most: high frequency noise shows the greatest negative correlation at 8 mm, while low frequency noise has a local maximum at 80 mm.

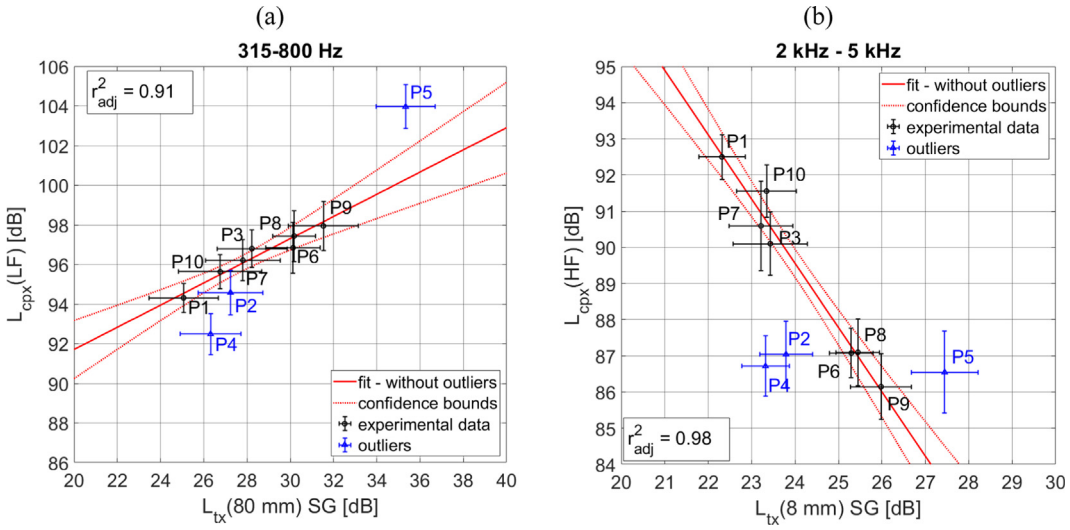

Fig. 12. Linear fit of data with exclusion of outliers.

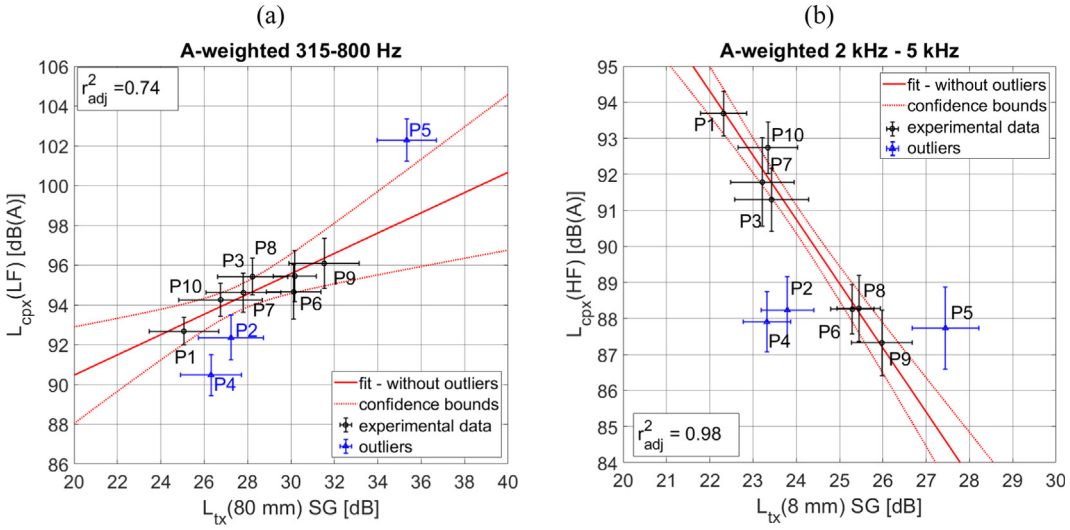

Fig. 13. A-weighted regressions.

Table 5
Regression parameters for A-weighed noise.

Frequency range	a	b	Adj. r^2
315–800 Hz	0.51 ± 0.12	71.4 ± 4.3	0.74
2–5 kHz	−1.78 ± 0.11	133.5 ± 2.7	0.98

4.5. Modelling of rolling noise

Modelling of rolling noise was performed using a linear regression with texture bands that correlate the most with noise, leading to the following equations:

$$L_{CPX}(HF) = a_{hf} L_{SG,tx}(8\text{mm}) + b_{hf} \quad (7)$$

where:

$L_{CPX}(HF)$ is noise level at high frequency,
$L_{SG,tx,8}$ is the SG texture level at 8 mm,
a_{hf} and b_{hf} are the regression parameters

and:

$$L_{CPX}(LF) = a_{lf} L_{SG,tx}(80\text{ mm}) + b_{lf} \quad (8)$$

where:

$L_{CPX}(LF)$ is the noise level at low frequency,
$L_{SG,tx,80}$ is the SG texture level at 80 mm,
a_{bf} and b_{bf} are the regression parameters.

Regression of Eqs. (7) and (8) was carried out using a robust regression with bi-square weighting function that takes into account uncertainty of experimental data.

Goodness-of-fit was evaluated calculating the adjusted coefficient of determination r^2_{adj}, intended to be an unbiased estimate of the coefficient of determination of the population, especially in small samples.

The linear regressions with the complete dataset containing ten surfaces are shown in Fig. 11.

Low frequency noise is apparently well described by the linear fit in Fig. 11(a), while the high frequency component in Fig. 11(b) underlines the presence of three outliers, namely P2, P4 and P5.

Regression parameters for Eqs. (7) and (8) are reported in Tables 3 and 4.

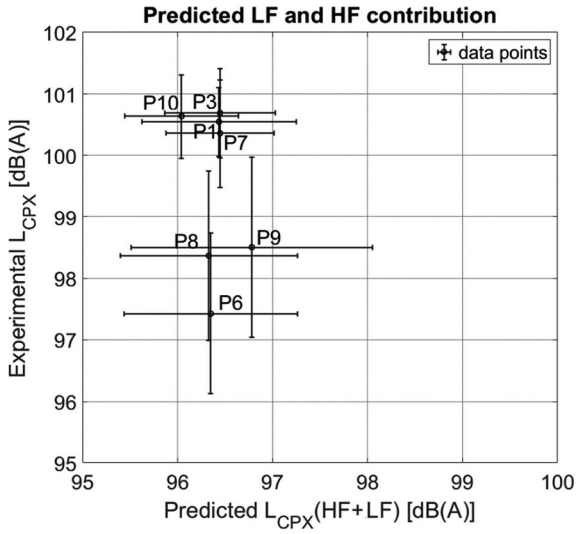

Fig. 14. Predicted low and high frequency contributions to broadband L_{CPX} vs experimental L_{CPX} data.

The elimination of the three outliers leads to Fig. 12(a) and (b). Data fits without outliers show higher adjusted r^2 values.

Based on the results of the linear regressions after the removal of the outliers, low frequency and high frequency noise can be modelled as:

$$L_{CPX}(LF) = 0.56L_{SG,tx}(80\ \text{mm}) + 80.5$$
$$L_{CPX}(HF) = -1.77L_{SG,tx}(8\ \text{mm}) + 132.2$$

Since CPX results are reported in A-weighted decibels, the same low frequency and high frequency levels defined in Eqs. (5) and (6) were recalculated adding A-weighting contribution for each frequency band A_{weight}:

$$L_{CPX}(A, LF) = \sum_{j=315}^{800} 10^{0.1(L_{CPX}(j)+A_{weight}(j))}$$
$$L_{CPX}(A, HF) = \sum_{j=2000}^{5000} 10^{0.1(L_{CPX}(j)+A_{weight}(j))}$$

A new regression was performed using these A-weighed variables. Regressions and the comparison with experimental data are shown in Fig. 13(a) and (b). The resulting goodness-of-fit reported in Table 5 show that A weighted low frequency noise is not described as well as the correspondent non-weighted quantity, while high frequency noise in unaffected by A-weighting.

A-weighted levels can be therefore modelled in a very similar way to non-weighted noise levels:

$$L_{CPX}(A,\ LF) = 0.51L_{SG,tx}(80\ \text{mm}) + 71.4$$
$$L_{CPX}(A,\ HF) = -1.78L_{SG,tx}(8\ \text{mm}) + 133.5$$

Despite the good values of the adjusted coefficient of determination, the CPX level resulting from the energetic sum of $L_{CPX}(A, LF)$ and $L_{CPX}(A, HF)$ does not yield information on the experimental CPX level, as shown in Fig. 14.

Therefore, while being able to describe low frequency and high frequency noise, the models presented lack predictive power on broadband L_{CPX}, since the contribution of the one third octave bands from 1 kHz to 1.6 kHz cannot be neglected.

5. Discussion

Correlation patterns in Fig. 9 show two distinct zones of correlation: a positive zone, which relates low frequency noise (315–800 Hz) with all texture bands, peaked at 80 mm, and a high frequency region (2000–5000 Hz), negatively correlated with road texture and with a minimum at 8 mm. The different behaviour can be explained analysing the different generation mechanisms that dominate the two regions: low frequency noise is caused by tyre vibrations, which is enhanced by higher texture components, while high frequency noise is due to aerodynamic mechanisms, which are suppressed in case deep valleys are present on the road profile. Both these aspects, however, lead to an increase of texture amplitude, and, in turn, of its spectrum.

Analysis in one-third octave bands shows that, for low frequency noise, the envelopment processes enhance correlation; however, correlation patterns at 10 mm is disrupted by Von Meier's algorithm, while the indenter model not only enhances correlation between texture and low frequency noise, but it also leads to a better determination of the couple of texture and noise bands with highest negative correlation in the high frequency region.

By observing the figures in Section 4.3, it is rather clear that VM acts as a smoothing filter, while SG algorithm preserves the shape of the profile down to a certain depth, and connects the edges with cubic polynomials. It is also interesting to notice that the gain of SG method offers less inter-quartile variation compared to VM algorithm, suggesting that SG algorithm offers a more stable procedure for tyre envelopment, less dependent on the road surface characteristics.

Low frequency sound levels, related to tyre vibrations, shows the strongest correlation at 80 mm for all methods adopted; however, the maximum value is obtained by the indenter's method (correlation coefficient $\rho = 0.93$).

High frequency sound level, caused by aerodynamic processes, has minimum negative correlation with envelopment performed according to the indenter's method at 8 mm ($\rho = -0.73$), which, despite being somewhat lower compared to the original profile, is still notably strong.

Nevertheless, Fig. 9 does not shed light on middle frequency noise (1000–1600 Hz). In fact, it is reasonable to assume that in this region a steady transition occurs from the positive correlation with the band centred at 80 mm to the negative correlation shown by high frequency noise at 8 mm.

Due to the lack of correlation in the middle frequency region between noise and road texture, modelling took place in the low frequency region, using a linear regression between L_{CPX} (*LF*) and L_{TX} (80 mm), and in the high frequency region, between L_{CPX} (*HF*) and L_{TX} (8 mm). Texture levels were calculated on enveloped profiles, using the indenter's method.

The three outliers pinpointed by the linear regression can be explained by taking into account issues that occurred during the laydown process, which caused not only significant changes in texture, but reasonably in other physical quantities that influence rolling noise, such as layer thickness, porosity and stiffness. The exclusion of the three outlier road surfaces from linear regression leads to high values of the adjusted coefficient of determination, which indicate a high goodness-of-fit.

Regression parameters are in accordance with literature: the slope $a_{80} = 0.51 \pm 0.12$ is remarkably close to the value 0.5 suggested by Sandberg for the Estimated Road Noisiness Level (ERNL) [9]. However, the same model used the texture level at 5 mm as an estimator of aerodynamic contribution to noise, with a slope of −0.25, slightly different compared to the slope $a_8 = -1.78 \pm 0.11$ obtained in this work. It appears therefore that the effect of envelopment is to increase the slope of high frequency noise as a function of texture.

The attempt to describe the broadband level as a function of low frequency and high frequency level did not bring any positive result, since tyre/road noise is dominated by levels around 1 kHz, which was not modelled in this work.

However, a hint of clustering of broadband CPX levels can be observed in Fig. 14, grouping P10, P3, P1 and P7 in one group and P6, P8 and P9 in another group. Since pavements within the cluster behave similarly in the frequency range from 1 to 1.6 kHz, it is clear that broadband L_{CPX} levels are extremely dependent on this contribution, rather than the low frequency and high frequency levels. This can be explained not only by the higher levels recorded, but also by the nature of A-weighting, which enhances frequencies around 1 kHz. It is interesting to notice, moreover, that the two different groups highlighted in Fig. 14 correspond to the two different production methods of rubberized surfaces. Indeed, as reported in Table 1, P1, P3, P7 are dry surfaces and, together with P10, form a single group in Fig. 14, while P6, P8 and P9 are wet road surfaces. Therefore, it is arguable that the production means could affect the acoustic performance of rubberized surfaces.

Therefore, the models proposed, while not being able to forecast broadband CPX levels, can describe low and high frequency levels in terms of road texture, thus shedding light upon the basic relations which link road texture to tyre/road noise.

6. Conclusions

This paper implemented a new approach for the evaluation of tyre/road noise, considering a tyre envelopment algorithm derived by road profile measurements.

A total of ten road surfaces were analysed in terms of CPX noise and texture levels. SG algorithm showed a distinct superiority compared to VM method in describing tyre deformation due to road texture and its relationship with rolling noise.

The results are comparable to previous studies, with the identification of two distinct patches of correlation: a positively correlated zone for low frequency emission and a negatively correlated region at higher frequencies.

The low frequency region, which showed the highest correlation at 80 mm, ranges from 315 to 800 Hz, while high frequency noise involves frequencies from 2000 to 5000 Hz and correlates the most at 8 mm. This has led to the definition of two indicators, a low frequency CPX level and a high frequency CPX level, which were described as a linear function of SG texture levels within the one-third octave bands, centred respectively at 80 mm and 8 mm.

Unfortunately, frequencies around 1000 Hz showed little correlation with road texture and its modelling was not performed. A multivariate linear regression did not yield results, since middle frequencies represent a transition zone from the positively correlated zone and the negatively correlated one.

Modelling noise in this region, therefore, requires deeper investigation and a better understanding of the physical phenomena underlying road tyre interactions.

Moreover, the presence of three outliers in the sample studied, due to other uncontrolled variables (laying conditions, temperature conditions of bitumen, etc.) could be reduced in the future ensuring a better standard level for laying process and homogeneity of production process.

Further research is needed to investigate the validity of the model and time-stability of the coefficients found in this work, by repeating measurements over a longer period of time.

Tyre envelopment algorithms also require deeper investigation, such as performing measurements at higher speeds in order to elaborate a speed-dependent indenter model.

An increase of the sample size could confirm the validity of the coefficients found for rubberized pavements, extending the model validity to other kinds of road surfaces. The selection of future samples, however, cannot be performed randomly, but should always be made ensuring that traffic and weather conditions are uniform within the sample, thus minimising their influence on the generation of tyre/road noise.

Declaration of Competing Interest

The authors declare that they have no known competing financial interests or personal relationships that could have appeared to influence the work reported in this paper.

References

[1] European Commission 2017. Report from the Commission to the European Parliament and the Council on the Implementation of the Environmental Noise Directive in accordance with Article 11 of Directive 2002/49/EC. COM/2017/0151 final.

[2] Muzet A. Environmental noise, sleep and health. Sleep Med Rev 2007;11(2):135–42.

[3] Hygge S, Evans GW, Bullinger M. A prospective study of some effects of aircraft noise on cognitive performance in schoolchildren. Psychol Sci 2002;13(5):469–74.

[4] Lercher P, Evans GW, Meis M. Ambient noise and cognitive processes among primary schoolchildren. Environ Behav 2003;35(6):725–35.

[5] Babisch W, Swart W, Houthuijs D, Selander J, Bluhm G, Pershagen G, et al. Exposure modifiers of the relationships of transportation noise with high blood pressure and noise annoyance. J Acoust Soc Am 2012;132(6):3788–808.

[6] Miedema HM, Oudshoorn CG. Annoyance from transportation noise: relationships with exposure metrics DNL and DENL and their confidence intervals. Environ Health Perspect 2001;109(4):409.

[7] Licitra G, Ascari E, Fredianelli L. Prioritizing process in action plans: a review of approaches. Curr Pollut Rep 2017;3(2):151–61.

[8] Ögren M, Molnár P, Barregard L. Road traffic noise abatement scenarios in Gothenburg 2015–2035. Environ Res 2018;164:516–21.

[9] Sandberg U, Ejsmont J. Tyre/road noise reference book. Kisa, Sweden: INFORMEX; 2002.

[10] Praticò FG. Roads and loudness: a more comprehensive approach. Road Mater Pavement Des 2001;2(4):359–77.

[11] Lee HW, Cho JR, Jeong WB. Numerical method for simulating tire rolling noise by the concept of periodically exciting contact force. Int J Automot Technol 2017;18(5):823–32.

[12] Winroth J, Kropp W, Hoever C, Beckenbauer T, Männel M. Investigating generation mechanisms of tyre/road noise by speed exponent analysis. Appl Acoust 2017;115:101–8.

[13] Li T, Burdisso R, Sandu C. Effect of rubber hardness and tire size on tire-pavement interaction noise. Tire Sci Technol 2017.

[14] Bravo T. An analytical study on the amplification of the tyre rolling noise due to the horn effect. Appl Acoust 2017;123:85–92.

[15] Kindt P, Berckmans D, De Coninck F, Sas P, Desmet W. Experimental analysis of the structure-borne tyre/road noise due to road discontinuities. Mech Syst Sig Process 2009;23(8):2557–74.

[16] Praticò FG. On the dependence of acoustic performance on pavement characteristics. Transp Res Part D: Transp Environ 2014;29:79–87.

[17] ISO 11819-2:2017 Acoustics - Measurement of the influence of road surfaces on traffic noise – Part 2: The close-proximity method.

[18] ISO 13473-2:2002 Characterization of pavement texture by use of surface profiles – Part 2: Terminology and basic requirements related to pavement texture profile analysis.

[19] Losa M, Leandri P, Licitra G. Mixture design optimization of low-noise pavements. Transp Res Rec: J Transp Res Board 2013;2372:25–33.

[20] ISO/TS 13473-4:2008 Characterization of pavement texture by use of surface profiles – Part 4: Spectral analysis of surface profiles.

[21] Licitra G, Cerchiai M, Teti L, Ascari E, Bianco F, Chetoni M. Performance assessment of low-noise road surfaces in the leopoldo project: comparison and validation of different measurement methods. Coatings 2015;5(1):3–25.

[22] ISO 13473-5:2009 Characterization of pavement texture by use of surface profiles Part 5: Determination of megatexture.

[23] Kim BS. Sound radiation due to tire tread vibration. JSME Int J Ser C 2003;46(2):675–82.

[24] Brinkmeier M, Nackenhorst U, Petersen S, Von Estorff O. A finite element approach for the simulation of tire rolling noise. J Sound Vib 2008;309(1–2):20–39.

[25] Klein P, Hamet JF. Road texture and rolling noise: An envelopment procedure for tire-road contact; 2004.

[26] Hamet JF, Klein P. Road texture and tire noise. In: Proc. InterNoise; August 2000. p. 178–83.

[27] Von Meier A, Van Blokland GJ, Descornet G. The influence of texture and sound absorption on the noise of porous road surfaces. In: Second International Symposium on Road Surface Characteristics, Berlin, Germany; June 1992.

[28] Goubert L, Sandberg U. Enveloping texture profiles for better modelling of the rolling resistance and acoustic qualities of road pavements. In: Symposium on Pavement Surface Characteristics (SURF), 8th, 2018, Brisbane, Queensland, Australia; May 2018.

[29] Licitra G, Moro A, Teti L, Del Pizzo A, Bianco F. Modelling of acoustic ageing of rubberized pavements. Appl Acoust 2019;146:237–45.
[30] Moro A, Teti L, Bianco F, Licitra G. Long Term Monitoring of Acoustic Performances of Rubberized Surfaces. In Rubberized Asphalt Asphalt Rubber (RAR) 2018; September 2018.
[31] Licitra G, Cerchiai M, Teti L, Ascari E, Fredianelli L. Durability and variability of the acoustical performance of rubberized road surfaces. Appl Acoust 2015;94:20–8.
[32] De León G, Del Pizzo A, Teti L, Moro A, Bianco F, Fredianelli L, Licitra G. Evaluation of Tyre/Road Noise and Texture Interaction on Rubberized and Conventional Pavements Using CPX and Profiling Measurements, manuscript submitted to Road Materials and Pavement Design; 2019.
[33] Licitra G, Teti L, Cerchiai M, Bianco F. The influence of tyres on the use of theCPX method for evaluating the effectiveness of a noise mitigation action based on low-noise road surfaces. Transp Res Part D: Transp Environ 2017;55:217–26.
[34] Del Pizzo A, Bianco F, Teti L, Moro A, Licitra G. A new approach for the evaluation of the relationship between road texture and rolling noise. In 25th International Congress on Sound and Vibration (ICSV25), Hiroshima, Japan; July 2018.
[35] Bendat JS, Piersol AG. Random data analysis and measurement procedures. 3rd ed. USA: John Wiley & Sons; 2000.
[36] ISO/TS 11819-3:2017 Acoustics – Measurement of the influence of road surfaces on traffic noise – Part 3: Reference tyres.
[37] Losa M, Leandri P, Bacci R. Empirical rolling noise prediction models based on pavement surface characteristics. Road Mater Pavement Des 2010;11(suppl. 1):487–506.